IET Radar Sonar and Navigation, Available online 20 July 2018
DOI:10.1049/iet-rsn.2018.5241

IET Research Journals

IET Journals
The Institution of Engineering and Technology

Bio-inspired Processing of Radar Target Echoes

ISSN 1751-8644
doi: 0000000000
www.ietdl.org

Krasin Georgiev [1,2] ✉, *Alessio Balleri* [1], *Andy Stove* [3], *Marc W. Holderied* [4]

[1] *Centre for Electronic Warfare, Information and Cyber, Cranfield University, Defence Academy of the UK, Shrivenham, SN6 8LA, UK*
[2] *Current affiliation: Department of Aeronautics, Technical University of Sofia, Sofia, Bulgaria*
[3] *Stove Specialties, Hove, E. Sussex, BN3 5NL, UK*
[4] *School of Biological Sciences, University of Bristol, BS8 1TQ, UK*
✉ *E-mail: krasin@tu-sofia.bg*

Abstract: Echolocating bats have evolved the ability to detect, resolve and discriminate targets in highly challenging environments using biological sonar. The way bats process signals in the receiving auditory system is not the same as that of radar and sonar and hence investigating differences and similarities might provide useful lessons to improve synthetic sensors. The Spectrogram Correlation And Transformation receiver (SCAT) is an existing model of the bat auditory system that takes into account the physiology and the neural organisation of bats that emit broadband signals. In this paper, we present a baseband receiver equivalent to the SCAT that allows an analysis of target echoes at baseband. The Baseband SCAT (BSCT) is used to investigate the output of the bat-auditory model for two closely spaced scatterers and to carry out an analysis of range resolution performance and a comparison with the conventional matched filter. Results firstly show that the BSCT provides improved resolution performance. It is then demonstrated that the output of the BSCT can be obtained with an equivalent matched-filter based receiver. The results are verified with a set of laboratory experiments at radio frequencies in high Signal to Noise Ratio (SNR).

1 Introduction

Bats use echolocation to sense the environment actively. Over a period of 50 million years, they have evolved an echolocation system that allows them to hunt for insects, forage for fruit or flower nectar and navigate in complex environments [1–5]. Similarly, modern radar (and sonar) systems rely on active sensing to support a variety of tasks that include detection and classification of targets, accurate localization and tracking, autonomous navigation and collision avoidance [6–8].

The basic principles of bat echolocation largely coincide with those of synthetic radar and sonar systems. Bats emit ultrasound echolocation calls and then listen for target echoes. By analysing the echo returns, they determine the presence of a target and, the echo time delay and the echo strength provide an indication of the target range and size, respectively. Similarly to radar, shifts in frequency due to the movement of a target (the so called Doppler effect) provide an indication of the target speed.

Despite these similarities, there are also some key differences to explore. Although both bats and synthetic sensors deploy frequency modulated waveforms, radar mostly use linear chirps while echolocation calls present non-linear frequency modulations often consisting of harmonics, e.g. hyperbolic chirps. Conventional radar rely on a small set of predetermined waveforms while bats diversify the transmitted waveform on a pulse to pulse basis by adapting the pulse width, the Pulse Repetition Frequency (PRF), the bandwidth and the waveform design [9]. In addition to this, it has been shown bats also use subtle changes of the "timbre" (i.e. the spectral content) of the sound and that this can bring information about the fine structure of a reflecting object (e.g. shape and the texture) [10, 11].

A key feature of echolocation is the ability of the bat to resolve highly overlapping echoes, from closely spaced targets or different target components, even when the degree of overlap is well beyond the range resolution achievable by a synthetic sensor using the same type of signals and a matched-filter. Behavioural experiments have demonstrated that frequency modulating (FM) bats are able to resolve two target spaced as little as 2 μs apart with a bandwidth of 80 kHz [12, 13], 1 μs with a bandwidth of 100 kHz [14] and 0.38 mm with 135 kHz [11]. This is less than one third of the corresponding nominal range resolution of a radar or sonar system, defined as the half power width of the matched-filter response to a point target [15]. The results of these biological experiments are compatible with the performance achieved by bats on a variety of tasks. There is biological evidence that the way bats process signals in the receiving auditory system is not equivalent to the matched filter used in radar systems. The Spectrogram Correlation And Transformation (SCAT) receiver is a model of the auditory system that was proposed by Saillant *et al.* for the bat *Eptesicus fuscus* [10]. It is a model that uses range information, a single receiver, and does not account for directional sensitivity. The SCAT was selected for further analysis because it is one of the most frequently referenced available models and because it is relatively simple and yet biologically plausible, as it provides a neural implementation at all stages.

While the aim of existing bat auditory system models [10, 16, 17] is to reproduce the acoustic images perceived by bats, there is no explanation on what exactly brings the performance improvement so it could be exploited in a technological system. Although the delay accuracy and resolution performance of the matched filter have been extensively investigated (e.g. [15] and [18]), there has been very little research in the existing literature to study the performance of bio-inspired models with radar signals.

The Baseband SCAT (BSCT) is a receiver that was developed based on the SCAT model to allow a mathematical treatment of the output of the SCAT and the processing of signals centred on very high carrier frequencies [19].

This paper investigates the output of the BSCT for two closely spaced scatterers and presents an analysis of range resolution performance and a comparison with the conventional matched filter receiver. The noise-free response of the BSCT receiver is found analytically for transmitted waveforms with a flat spectrum, such as Linear Frequency Modulated (LFM) and stepped frequency signals, and this shows that the BSCT can provide improved range resolution performance than the matched filter. A description of the algorithm is also available in [20]. It is then demonstrated that the output of the BSCT can be obtained with an equivalent matched-filter based receiver and this is a key contribution of this paper. The theoretical

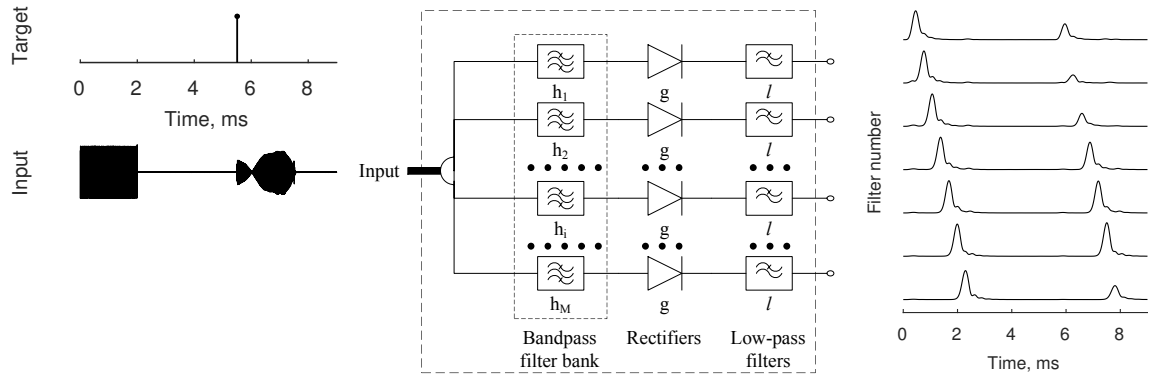

Fig. 1: Cochlear block of the SCAT receiver. The filter bank consists of $M = 81$ bandpass filters h_i with central frequencies from 20 kHz to 100 kHz. A rectifier and a Butterworth low-pass filter follow after each bandpass filter. Both the emitted call and the received echo are processed. The waveform is a 2 ms linear chirp. The echo consists of two reflections delayed by 18 μs. The output is shown on the right – multiple channels of low frequency signals.

results are verified with a set of laboratory experiments at radio frequencies with non-ideal distributed targets in high Signal to Noise Ratio (SNR).

2 Description of the Spectrogram Correlation and Transformation Model

The SCAT model consists of three blocks called the cochlear block, the temporal (spectrogram correlation) block and the spectral (spectrogram transformation) block that model the peripheral and the central auditory system of FM bats [10].

2.1 Cochlear block

In the cochlear block, the received wideband signal is filtered to generate multiple parallel low frequency signals, so further processing by the neural system is possible (Fig. 1). The cochlear block is modelled with a bank of 81 Butterworth band-pass filters of order 10 and bandwidth $B = 4$ kHz. Each filter is followed by a signal rectifier and a 3 kHz bandwidth low-pass filter to extract the envelope of the narrowband channels.

The central frequencies f_i of the band-pass filters span the bandwidth between 20 kHz and 100 kHz and are arranged in a hyperbolic scale with $f_i = 1/p_i$, where the central period p_i changes linearly from 10 μs to 50 μs with increments δp of 0.5 μs. With a 4 kHz bandwidth, at the lower-frequency end of the spectrum the filters overlap (channel spacing about 2.5 kHz) but at the upper end the spectrum is slightly undersampled (channel spacing about 5 kHz).

In the literature, some modified versions of the original SCAT have been proposed, which differ in how the initial splitting of the signal into frequency channels is carried out. For example, the bank of constant bandwidth Butterworth filters may be replaced by gammatone filters with frequency dependent bandwidths [17] or Gaussian chirplets with carrier frequencies compatible with the emission sweep rate [16]. Additional non-linear transformations have been proposed to account for the non-linear interactions within the organ of corti [17]. An excellent review of auditory system models is presented in [21].

2.2 Temporal block

The purpose of the temporal block is to estimate the time delay between the call and the echo based on the output of the cochlear block. It consists of a set of tapped delay lines to carry out a "dechirping" of the signal by adding appropriate delays to each frequency channel. Simultaneous activity in multiple channels is detected by a set of coincidence detection neurons and is a sign of the target presence.

The temporal block does not require a direct copy of the transmitted signal. However, the transmitted waveform design is key to determine the delays applied at each tapped delay line. For a typical bat call, the temporal block provides a compression of the input signal from several milliseconds (0.5-15 ms) to several hundreds microseconds (200-300 μs) as the impulse response of 4 kHz filters is relatively wide. Therefore, the temporal block alone provides information on the location of the targets with a relatively low range resolution, compared to that obtainable with standard pulse compression techniques. High range resolution, instead, is achieved in the spectral block.

2.3 Spectral block

The spectral block is responsible for extracting the fine structure of the target. It is used to detect and measure the delay between highly overlapping echoes, which cannot be resolved by the temporal block [10].

Each target detected by the temporal block is processed by the spectral block separately. The output signal of each frequency channel is integrated for a specific time interval (about 350 μs [10]). The output of the integration represents the frequency spectrum of the return signal from the target. It is next normalised by the interference pattern of the emitted call to get a target signature in the frequency domain. This is needed to compensate for the hyperbolic distribution of the energy when hyperbolic FM waveforms are used.

The spectral block exploits the interference pattern between overlapping echoes, which results in the suppression or amplification of the power of the output of some of the filters of the cochlear block. The original SCAT propose the so called "voting mechanism" to transform the echo spectrum back onto the time axis. It is a modified inverse cosine transform suitable for hyperbolic frequency sampling. A "pattern-matching" interpretation of the transformation of spectral interference patterns into fine delays is proposed in [22]. Other studies argue that time domain reconstruction of the target image is not necessary [11, 14, 17]. More recent developments of the SCAT receiver propose a mechanism to extract the spectral zeroes locations and then feed them to a neural network to reconstruct the target shape on the range axis [23].

3 The Baseband SCAT receiver (BSCT)

A baseband equivalent of the spectrogram transformation receiver, accounting for the Cochlear and the Spectral blocks, is proposed that can treat analytical input signals at baseband. It is also applicable to RF signals at very high frequencies (bandpass signals) which are converted to low frequency complex signals (baseband signals). Down-conversion to baseband is essential to digitise bandpass signals meeting the Nyquist criterion and, it also provides analytical advantages as signals can be represented in a much simpler complex form.

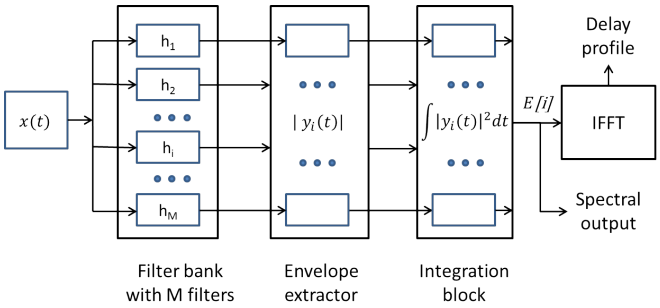

Fig. 2: BSCT spectral processing diagram The model input $x(t)$ is an analytical signal. It is passed through filter bank of M complex bandpass filters h_i. The absolute value of each filter output y_i is squared and integrated over time to get the energy $E[i]$ of the corresponding frequency

Let us consider a filter bank of M filters with central frequencies $f_i, i = 0 \dots M-1$ and bandwidth B. If the filters have all the same design, the Fourier transform $H_i(f)$ of the impulse response $h_i(t)$ for the i-th filter can be obtained by shifting in frequency a baseband (low-pass) filter response $h(t)$ as

$$h_i(t) = h(t)e^{j2\pi f_i t} \tag{1}$$

$$H_i(f) = H(f - f_i) \tag{2}$$

where $H(f)$ is the Fourier transform of $h(t)$. The response of the i-th filter is the convolution between the filter impulse response and the input signal $x(t)$

$$y_i(t) = x(t) * h_i(t) \tag{3}$$

The rectifiers and the low-pass filters that follow each bandpass filter of the original cochlear block (Fig. 1) are replaced with an ideal amplitude extractor, so that the envelope of the bandpass filtered signal can be modelled with the amplitude of the signal $y_i(t)$ (Fig. 2). The equivalence to the original SCAT was demonstrated experimentally in [19]. In the spectral block, the total energy of the output of each filter is computed by integration (Fig. 2). In order to separate the spectral signature of multiple groups of scatterers, the integration is limited to an interval around the location of the group of echoes under consideration so that each group can be analysed separately. The group locations for each frequency are extracted by the temporal block.

When only a single group of scatterers is present, the temporal block can be ignored and the output of the spectral block can be obtained by integrating the whole filter output

$$\begin{aligned} E[f_i] = E[i] &= \int_{-\infty}^{\infty} |y_i(t)|^2 \, dt = \int_{-\infty}^{\infty} |Y_i(f)|^2 \, df \\ &= \int_{-\infty}^{\infty} |X(f)|^2 \, |H_i(f)|^2 \, df \end{aligned} \tag{4}$$

When all narrow-band filters in the filter bank have a perfectly flat frequency response over a bandwidth B, i.e.

$$H_i(f) = \text{rect}\left(\frac{f - f_i}{B}\right) \tag{5}$$

where

$$\text{rect}(f) = \begin{cases} 1, & |f| \le \frac{1}{2} \\ 0, & \text{otherwise} \end{cases}$$

the filter bank spectral output is

$$E[i] = \int_{f_i - B/2}^{f_i + B/2} |X(f)|^2 \, df \tag{6}$$

Eq. (6) shows the spectrogram transformation provides the signal spectral energy of the input signal integrated over a bandwidth B around the central frequencies f_i. This is equivalent to the Daniell spectral estimation method for appropriate selection of B [24]. Finally, the sequence $E[i]$ is transformed into the time domain to obtain the output signal of the spectral block. Assuming the central frequencies f_i are linearly spaced at baseband, this transformation can be obtained with an Inverse Fast Fourier Transform (IFFT).

4 Response of the BSCT to two closely spaced ideal reflectors

We study the response of the BSCT to the echo from two closely spaced ideal point reflectors in order to investigate the range resolution properties of the model and to allow a comparison with the matched-filter. When two ideal targets are present, the complex envelope of the input signal $x(t)$ is the sum of two delayed replicas of the complex envelope of the transmitted signal $x_C(t)$

$$x(t) = x_C(t - t_1)e^{-j2\pi f_0 t_1} + x_C(t - t_2)e^{-j2\pi f_0 t_2} \tag{7}$$

where t_1 and t_2 are the time-delays of the echo from the first and second target, respectively, and f_0 is the carrier frequency. For simplicity of notation, the difference between the two delays will be denoted as $\tau = t_2 - t_1$.

The Fourier transform of $x(t)$ can be written as a function of the Fourier transform $X_C(f)$ of the signal $x_C(t)$ as

$$\begin{aligned} X(f) &= X_C(f)e^{-j2\pi(f+f_0)t_1} + X_C(f)e^{-j2\pi(f+f_0)t_2} \\ &= X_C(f)e^{-j2\pi f^I t_1} e^{-j\pi f^I \tau} 2\cos\left(\pi f\tau + \frac{\psi_\tau}{2}\right) \end{aligned} \tag{8}$$

and its energy spectral density is

$$\begin{aligned} |X(f)|^2 &= |X_C(f)|^2 \, 4\cos^2\left(\pi f\tau + \frac{\psi_\tau}{2}\right) \\ &= 2\,|X_C(f)|^2 \left[\cos(2\pi f\tau + \psi_\tau) + 1\right] \end{aligned} \tag{9}$$

where $f^I = f + f_0$ is the frequency before down-conversion and $\psi_\tau = 2\pi\tau f_0$ is the phase of the cosine wave after down-conversion.

Let us assume that the transmitted signal $x_C(t)$ is a Linearly Frequency Modulated chirp (LFM) with a bandwidth B_C and duration T of the form

$$x_C(t) = e^{j\pi\gamma t^2} \, \text{rect}\left(\frac{t}{T}\right) \tag{10}$$

where $\gamma = B_C/T$ is the chirp rate. The Fourier transform of the chirp

$$\begin{aligned} X_C(f) &= \int_{-\infty}^{\infty} x_C(t)e^{-j2\pi ft} dt \\ &= \int_{-T/2}^{T/2} e^{-j2\pi\left(ft - \frac{\gamma t^2}{2}\right)} dt \end{aligned} \tag{11}$$

for large time-bandwidth products ($B_C T >> 1$), after the stationary phase approximation [25], can be written as

$$X_C(f) = \sqrt{\frac{1}{\gamma}} \cdot e^{-j\pi\frac{1}{\gamma}f^2} e^{j\frac{\pi}{4}} \, \text{rect}\left(\frac{f}{B_C}\right) \tag{12}$$

The result consists of a linear chirp on the frequency axis over the band B_C. From (9), the energy spectral density of the return $x(t)$

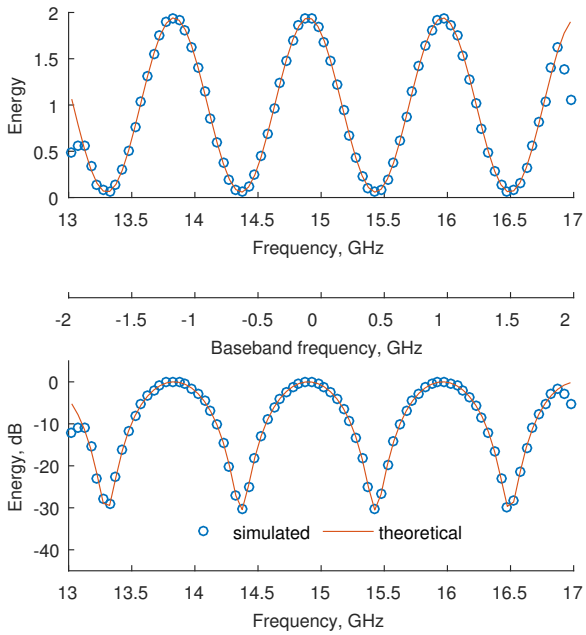

Fig. 3: Model output, energy E_E by filter i, $i = 1 \ldots 80$, $B = 0.2$ GHz, for two scatterers separated by 0.141 m. Based on simulated input and the derived theoretical solution in (14). The linear scale is used to emphasize the sinusoidal pattern and the logarithmic – the zeroes locations

from two scatterers can be written as

$$|X(f)|^2 = \frac{2}{\gamma} \cdot [\cos(2\pi f\tau + \psi_\tau) + 1] \cdot \mathrm{rect}\left(\frac{f}{B_C}\right) \tag{13}$$

and the output is

$$\begin{aligned} E_E[i] &= \frac{2}{\gamma} \int_{f_i - B/2}^{f_i + B/2} [\cos(2\pi f\tau + \psi_\tau) + 1]\, df \\ &= \frac{2B}{\gamma} [\mathrm{sinc}(\tau B) \cos(2\pi\tau f_i + \psi_\tau) + 1] \end{aligned} \tag{14}$$

for $|f_i| \leq (B_C - B)/2$, where $\mathrm{sinc}(x) = \sin(\pi x)/(\pi x)$. For $|f_i| \geq (B_C + B)/2$, $E_E[i] = 0$.

Equation (14) shows that the spectral output of the BSCT is the sum of a sinusoid and a constant and that the frequency of the sinusoid is exactly the time spacing between the targets τ. We will further refer to the spectral output as a frequency profile.

Figure 3 shows an example of a frequency profile corresponding to 80 filters with central frequencies distributed linearly between -2 GHz and 2 GHz and with a 200 MHz bandwidth. The simulations are relative to a step frequency signal, a central frequency of 15 GHz and a target spacing of 0.141 m.

The Inverse Fourier transform of the frequency profile $E_E(f)$, assuming rectangular windowing over the bandwidth B_C, is

$$\begin{aligned} \mathcal{F}^{-1}[E_E] &= 2\frac{B}{\gamma}\mathcal{F}^{-1}\left[\mathrm{rect}\left(\frac{f}{B_C}\right)\right] * \\ &* \mathcal{F}^{-1}\left[\mathrm{sinc}(B\tau)\cos(2\pi f\tau + \psi_\tau) + 1\right] \\ &= 2\frac{BB_C}{\gamma}\Big[\mathrm{sinc}(B_C t) + \\ &+ \frac{be^{j\psi_\tau}}{2}\mathrm{sinc}(B_C(t-\tau)) + \frac{be^{-j\psi_\tau}}{2}\mathrm{sinc}(B_C(t+\tau))\Big] \end{aligned} \tag{15}$$

where $b = \mathrm{sinc}(B\tau)$.

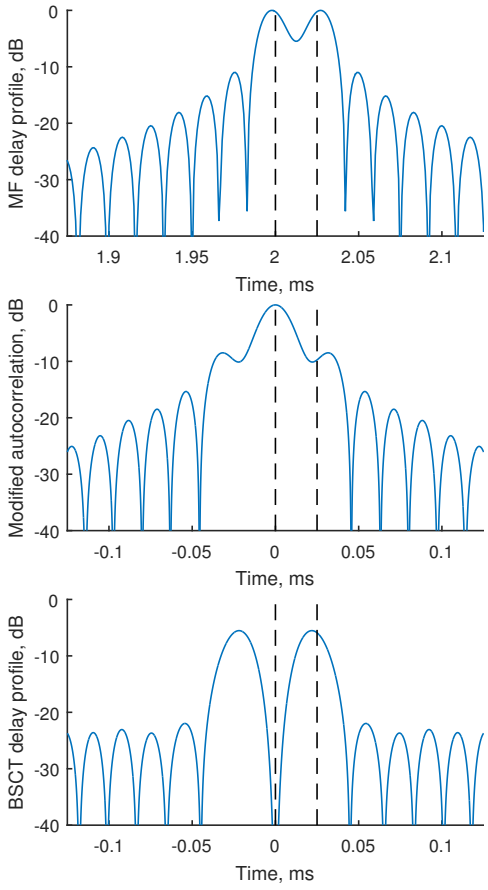

Fig. 4: Matched filter compared to BSCT and the effect of the zero lobe suppression

4.1 Central lobe suppression

Without further processing the time resolution of two closely located scatterers of the bio-inspired spectrogram transformation is the same as the resolution achieved by the matched filter. The distance between the sinc functions is τ as for the matched filter and the width of the lobes in the time domain at -3 dB is the reciprocal of the bandwidth of the signal (or that of the filter bank if it is less):

$$\Delta\tau = \frac{1}{B_C}$$

However, the central lobe does not depend on the position of the targets and can be suppressed to double the distance between the two lobes at $\pm\tau$. If the suppression of the central lobe is achieved then the distance between the two sinc functions is increased from τ to 2τ and the functional range resolution is improved so that two targets at half the range separation can be resolved (Fig. 4). Furthermore, because the resulting representation is symmetrical, we can imagine folding it back on itself so there is essentially only a single peak. This means that measuring the relative distance between two targets has been made as simple as measuring the range to a single target [6, Sec. 3.1]. There are a few approaches that can be considered to remove the central lobe. One is to use the knowledge of the transmitted signal parameters and remove a suitably scaled version of the sinc and another is to remove the average value of the spectral energy over the bandwidth before taking the inverse Fourier transform [22].

Removing the mean of (14) leads to

$$E_{E'}(f) = E_E(f) - \frac{1}{B_C}\int_{-\frac{B_C}{2}}^{\frac{B_C}{2}} E_E(f)df \cdot \mathrm{rect}\left(\frac{f}{B_C}\right)$$
$$= 2\frac{1}{\gamma}\cdot\Big[\mathrm{sinc}(\tau B)\cos(2\pi f\tau+\psi_\tau) -$$
$$-\mathrm{sinc}(\tau B)\,\mathrm{sinc}\left(\tau B_C\right)\cos\psi_\tau\Big] \quad (16)$$

Equation (16) shows that, with this method, the constant component in $E_E(f)$ is still present but reduced (16).

4.2 Interpretation of the BSCT profiles

Unlike the matched filter, the BSCT is non-linear and its output encodes directly the spacing between the scatterers and not the absolute range of the targets. The problem of measuring the distance between the targets is converted into a problem of measuring the range to a single target. As the representation is symmetrical, there is a second peak at negative delays but the peaks interfere less than the peaks produced by a matched filter because the separation is double.

We will further refer to the fine delay profile of the BST as a spacing profile to emphasise the nature of the information conveyed, i.e. not the absolute location of the scatterers but the spacing between them. Because the BSCT is non-linear, a peak is generated for each possible spacing between the scatterers. To illustrate this, we can investigate the most simple case of three scatterers for which

$$x(t) = x_C(t-t_1)e^{-j2\pi f_0 t_1} + x_C(t-t_2)e^{-j2\pi f_0 t_2} + x_C(t-t_3)e^{-j2\pi f_0 t_3} \quad (17)$$

and

$$X(f) = X_C(f)e^{-j2\pi(f+f_0)t_1} + X_C(f)e^{-j2\pi(f+f_0)t_2} + X_C(f)e^{-j2\pi(f+f_0)t_3}$$
$$= X_C(f)e^{-j2\pi f^I t_1}\left(1+e^{-j2\pi f^I(t_2-t_1)}+e^{-j2\pi f^I(t_3-t_1)}\right) \quad (18)$$

The energy spectral density $|X(f)|^2$ is

$$|X(f)|^2 = X(f)X(f)^*$$
$$= |X_C(f)|^2\left(1+e^{-j2\pi f^I\tau_{21}}+e^{-j2\pi f^I\tau_{31}}\right)\cdot \left(1+e^{-j2\pi f^I\tau_{21}}+e^{-j2\pi f^I\tau_{31}}\right)^* \quad (19)$$
$$= 2\,|X_C(f)|^2\Big(\cos(2\pi f^I\tau_{21})+\cos(2\pi f^I\tau_{31}) + \cos(2\pi f^I\tau_{32})+3/2\Big)$$

where τ_{ij} is the delay between the scatterer i and scatter j. This can be compared to the corresponding equation for two scatterers (9). Each pair of scatterers is represented by a cosine. All derivations from previous sections can be repeated here. The Inverse Fourier transform will convert each cosine to a positive and a negative peak at $\pm\tau_{ij}$ on the time axes. A similar analysis was presented in [22, 26]. The conclusion was that the spectral block generates spurious delay estimates or "ghost peaks" when more than two echoes are present. This is an inherent property of the spacing profile concept.

As for the case of two targets, even for the general case of multiple targets, the frequency profile of the BSCT (6) can be compared to the Daniell spectral estimation method [24]. The IFFT of the spectral energy density is the autocorrelation function (ACF) of the signal. Because the BSCT frequency profile represents the spectral energy of the target return, the BSCT spacing profile can be considered a modified autocorrelation.

5 Equivalent matched filter based receiver

In this section, we demonstrate that when the transmitted waveform has a flat frequency response, e.g a linear chirp or a stepped frequency waveform, the output of the BSCT receiver can be also obtained with a typical receiver that employs a matched filter.
Let us consider the two closely spaced targets that produce the echo signal $x(t)$ of (7). If the receiver consists of a filter matched to the waveform $x_C(t)$, the output of the matched filter $x_M(t)$ is

$$x_M(t) = x(t) \star x_C(t) \quad (20)$$

and its spectrum is

$$X_M(f) = X(f)X_C^*(f)$$
$$= X_C(f)e^{-j2\pi f^I t_1}e^{-j\pi f^I\tau}2\cos(\pi f^I\tau)X_C^*(f) \quad (21)$$
$$= 2\,|X_C(f)|^2\cos(\pi f^I\tau)\cdot e^{-j2\pi f^I t_1}e^{-j\pi f^I\tau}$$

We can compare the above equation with (8) and see that the only difference is that the waveform $X_C(f)$ is replaced by its magnitude squared $|X_C(f)|^2$. For a linear chirp with a large time-bandwidth product, the signal spectrum is flat as in (12) and

$$X_M(f) = \frac{2}{\gamma}\cos(\pi f^I\tau)\mathrm{rect}\left(\frac{f}{B_C}\right) \quad (22)$$

We observe that, if the signal whose spectrum is the energy spectral density at the output of the matched filter is passed through a bank of filters with a flat response, the energy of the signal at the output of each filter is

$$E_M[i] = \int_{f_i-B/2}^{f_i+B/2}|X_M(f)|^2\,df$$
$$= \frac{2B}{\gamma^2}\cdot[\mathrm{sinc}(B\tau)cos(2\pi f_i\tau+\psi_\tau)+1] \quad (23)$$

This is equivalent to taking the energy spectral density at the output of the matched filter and calculate the energy contained in each subband B. The result is exactly a scaled version of the BSCT output in (14).

This results show that the BSCT resolution can be obtained using existing receivers based on the matched filter and that improvements are only down to a software modification of the receiver. The matched filter will still be used to maximise the signal to Noise Ratio (SNR) and detect group of closely spaced scatterers. Each group can then be processed independently as described above to resolve targets within the group with a higher range resolution.

6 Experimental set up

An experiment was set to validate the range resolution properties of the BSCT model at Radio Frequency (RF). Measurements were performed from 13 GHz to 17 GHz using a Vector Network Analyzer (VNA) (MS46322A, Anritsu) and two 5x4 cm horn antennas. The VNA provides a measurement of the frequency response of a target sampled at constant frequency intervals by implementing a stepped frequency waveform with a flat spectrum. The step frequency Δ_F was 250 kHz so the recorded sequence consisted of $N = 16000$ data points. High Range Resolution Profiles (HRRPs) were obtained by taking an IFFT of the output data.

The two closely spaced targets used in the experiments were two identical vertical rods with a diameter of 0.006 m and a length of 0.75 m. The rods were placed on a turntable (LT360EX, LinearX Systems, Battle Ground, WA, USA) rotating with a step angular resolution of 1 degree. The transmitting and receiving antennas were

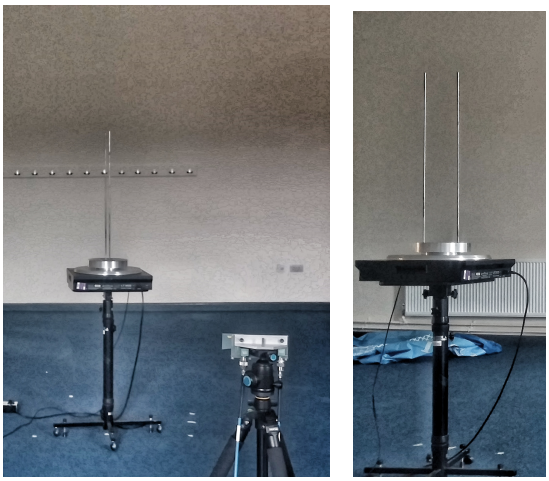

(a) Two vertical rods photos at 90 degrees aspect angle

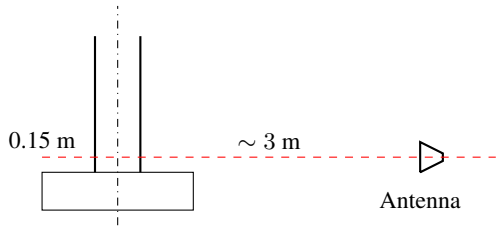

(b) Two vertical rods arrangement at 90 degrees aspect angle

Fig. 5: Experimental setup

placed at a distance of 3 m from the turntable centre of rotation and positioned at a height of approximately 1.1 m above the floor level and 0.04 m above the level of the turntable surface. This resulted in the receiving antenna being in the near-field scattering region of the targets. Rotating the turntable allowed the analysis of the output of the BSCT for values of radial spacing between the scatterers ranging between 0 and 0.150 m. A measurement of the background was taken for each aspect angle and removed from the data before processing. A photo and a diagram of the experimental setup is shown in Fig. 5 for a 90-degrees aspect angle, that is for the geometry corresponding to the maximum distance of the two rods with respect to the radar.

Simulated data mirroring the experiments were generated to allow a comparison between experiments and simulations.

7 Experimental results

The bio-inspired BSCT was applied to the RF data and the output was compared with that of the matched filter.

Following the approach in [6], the BSCT results were compared with the nominal resolution δ_R, defined as the half power width of a point target response of the matched filter (i.e. the reciprocal of the signal bandwidth appropriately scaled when transformed into distance). The BSCT was implemented and applied to the real data as follows:

1. obtain the range profile by taking an Inverse Fast Fourier Transform (IFFT) of the VNA data $X_M(f)$ after background removal;
2. detect the targets and obtain the approximate range (about 3 m in our setup);
3. isolate the reflections from the targets by zeroing the range profile outside the interval $[x_1, x_2]$ (we used $x_1 = 2$ m and $x_2 = 4$ m);
4. calculate the frequency response of the targets by applying a Fast Fourier Transform (FFT);

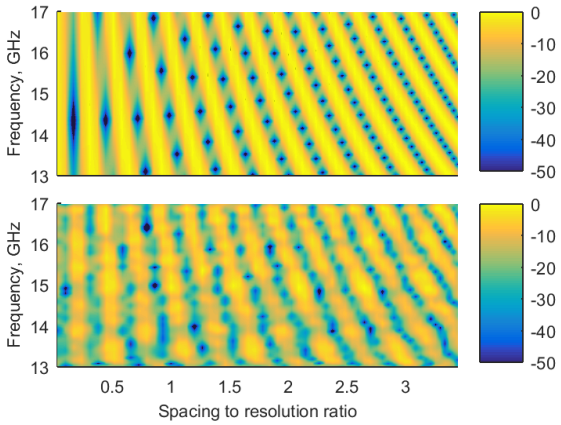

Fig. 6: BSCT frequency profiles for simulated data and for the two vertical rods (from top to bottom). The colour bar encodes the energy in dB.

5. calculate the spectral energy by taking the magnitude squared of the frequency response of the targets;
6. average the spectrum over small intervals centred on the frequencies of interest to obtain the frequency profile $E_M(f)$. We averaged over $M = 100$ samples for $K = 160$. The frequencies were linearly spaced over the measurement band (13–17 GHz). This corresponds to a bandpass filter bandwidth $B = M \times \Delta_F = 25$ MHz.

The first two steps implement a standard matched filter, provide the compressed signal in the time domain and correspond to the temporal block of the SCAT. The following two steps are used to isolate the closely spaced targets and calculate their frequency response. This corresponds to the limited integration time of the filter output in the original SCAT. The spectrogram transformation is implemented in the last two steps. The number of central frequencies K was selected so to be of the same order as the number of filters in the original SCAT.

The experimental BSCT frequency profiles as a function of the normalised target spacing, that is the ratio between the distance between the two rods at each turntable step and the nominal resolution, are shown in Fig. 6 together with the corresponding simulated data. Results show that the general shape and, in particular, the location of the zeroes are preserved between the experiments and the simulations. This indicates that the interference pattern of the BSCT is robust to real measurements, especially considering that the two rods are not ideal point targets. This corroborates the results in [27] but for data obtained with a transmitted waveforms with the same energy for all geometries.

The BSCT spacing profile was then obtained with the following steps:

7. subtract the average from the frequency profile to suppress the central sinc function of the response;
8. zero-pad to achieve an appropriate time (range) sampling period Δ_T ($\Delta_R = c\Delta_T/2$).

$$N_{\mathrm{FFT}} = \frac{K}{B_C \Delta_T} \tag{24}$$

9. apply the IFFT;

Fig. 7 shows the BSCT spacing profiles as a function of the normalised target spacing for the experimental data (Fig. 7d) and the corresponding simulations (Fig. 7b). These are compared with the matched filter range profiles with a SNR of approximately 30 dB in Fig. 7c and Fig. 7a. The amplitude of the profiles is colour coded in dB and results are presented for all normalised spacings starting from a 0-degrees aspect angle (that is with the two rods at the same distance from the radar). A comparison between the simulation results (Fig. 7a and Fig. 7b) shows that when the two rods

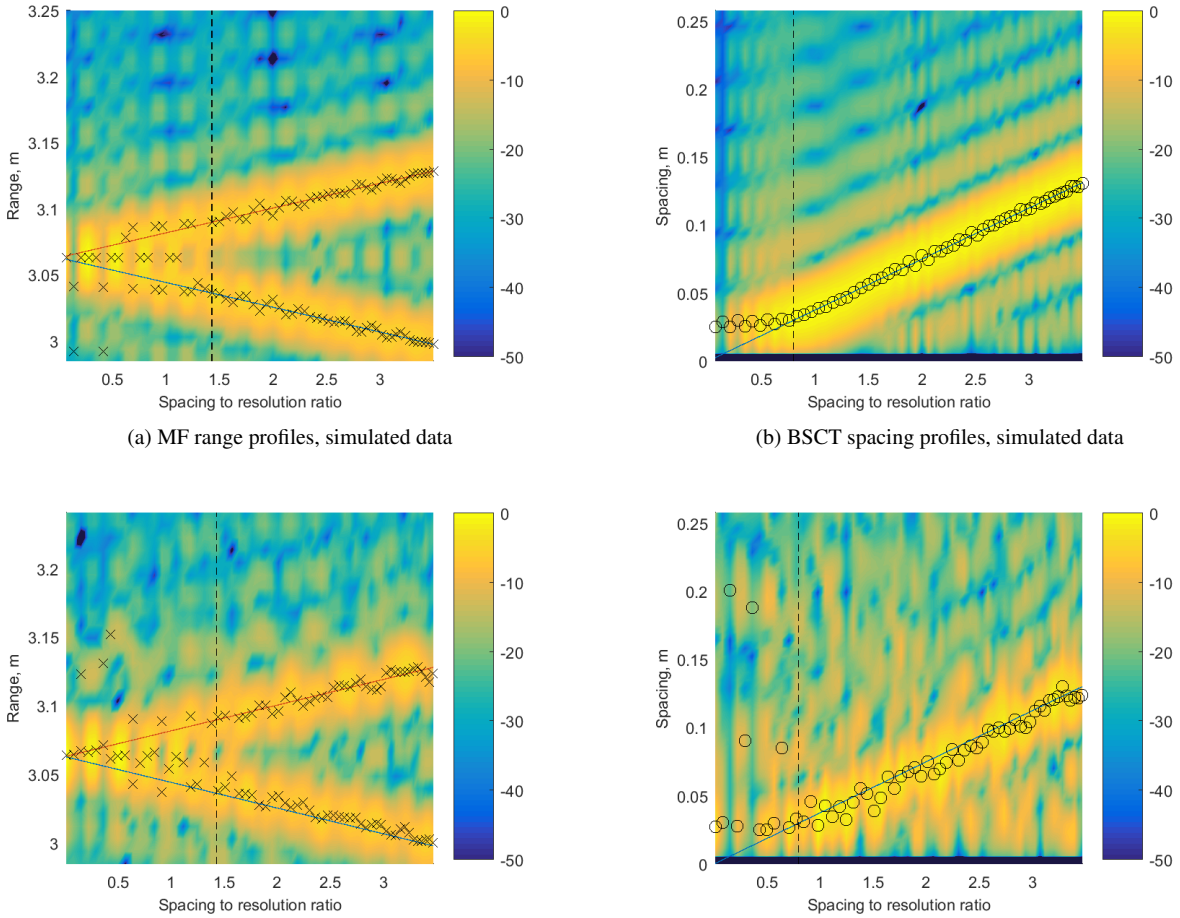

(a) MF range profiles, simulated data

(b) BSCT spacing profiles, simulated data

(c) MF range profiles, measurements of two rods

(d) BSCT spacing profiles, measurements of two rods

Fig. 7: Range profiles as a function of the separation between the scatterers. The signal bandwidth is 4 GHz and the SNR after pulse compression is approximately 30 dB. In the spectrogram transformation based approach the profile encodes the spacing between the scatterers. From the matched filter we get the absolute position of the scatteres.

are resolvable in range, as expected, the output of the matched filter for each normalised spacing consists of two peaks. These originate the two lines in the diagram when the normalised spacing is varied. The peak locations of the output of the matched filter are marked with crosses and provide an estimate of the true range of each scatterer. These were obtained with a standard peak detection algorithm using a threshold calculated as a function of the mean signal power and the standard deviations of the background noise, followed by a three point parabolic interpolation. Only peaks isolated of above 3 dB were considered. The two lines in the diagram represent the true range of the two rods from the radar. Results show that for the matched filter the two rods are resolvable for normalised spacings above 1.4 (the point of failure is indicated with a dashed line). Fig. 7b shows the corresponding results for the BSCT spacing profiles. The peak locations of the BSCT spacing profiles are marked with circles and provide an estimate of the true separation between the scatterers. Results show that the BSCT provides a correct estimate of the target spacing above less than 0.8. The results obtained with the real data are shown in Fig. 7c and Fig.7d. These are in a very good agreement with the simulation results and corroborate that the BSCT can provide a correct estimate of the spacing for lower values of the normalised spacing between the targets than the matched filter.

To allow a further comparison, the output of the matched filter was converted into the distance between the two targets by taking the difference between the peaks of the response. When the matched filter produced a single peak the distance was set to zero. The results of the comparison as a function of the normalised spacing are shown for both the simulations and the experiments in Fig. 8. In the figures, the BSCT spacing estimates are indicated with circles and those from the matched filter with crosses. The horizontal dotted line is the nominal resolution. Results show that, when the distance between the two rods decreases below about $1.5\delta_R$, the peaks of the matched filter merge. The BSTC instead can resolve the targets and provide an estimate of their distance up to less than $0.8\delta_R$. The range resolution is improved by nearly a factor of two.

8 Conclusion

A baseband receiver was proposed that allows an analytical treatment of the output of a SCAT-like processing and that can also be applied to RF signals. The output of the BSCT was derived analytically for two closely spaced scatterers and compared with that of a conventional matched filter. Results have shown that a bat-inspired spectrogram transformation can provide better range resolution performance than that of a matched filter output envelope. The problem of measuring the relative distance between two targets is converted to a problem of measuring the range to a single target. The robustness of the BSCT receiver for radio frequency signals and real targets was demonstrated experimentally. The enhanced resolution of two scatterers was confirmed. Furthermore, the paper shows that the algorithm can be applied after the matched filter and, as such, its implementation only requires a software addition and retains the performance of traditional processing at the very least.

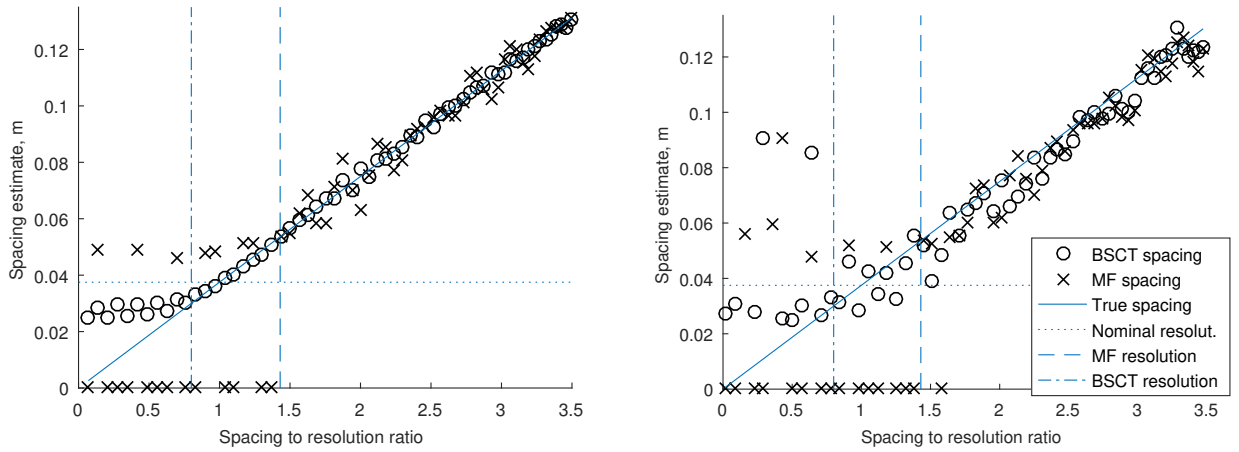

(a) Simulated target

(b) Vertical rods

Fig. 8: Estimated spacing as a function of the normalised spacing between the scatterers. The signal is a linear chirp with bandwidth 4 GHz and the SNR is approximately 30 dB. The nominal resolution limit is shown as dotted line. The dashed lines are positioned at normalised spacings 0.8 and 1.43. The physical target consists of two vertical rods on a turntable

Future work should investigate the performance of the BCST algorithm for targets with a significantly different Radar Cross Section (RCS) as well as analyse the performance of the algorithm as a function of the SNR to assess the effects of the non-linearity of the system when the noise power is high. This paper has focussed on studying the performance of the physical receiver design prior to any potential advanced signal processing. However, as super resolution techniques can be applied to the output of the matched filter, similarly, one can think to investigate their application to the output of the BSCT to further improve the performance.

Acknowledgment

Krasin Georgiev's work was supported by Cranfield Defence and Security under the CDS PhD bursary scheme.

9 References

1 Geipel, I., Jung, K., Kalko, E.K.V.: 'Perception of silent and motionless prey on vegetation by echolocation in the gleaning bat micronycteris microtis', *Proceedings of the Royal Society of London B: Biological Sciences*, 2013, **280**, (1754)

2 von Helversen, D.: 'Object classification by echolocation in nectar feeding bats: size-independent generalization of shape.', *Journal of comparative physiology A, Neuroethology, sensory, neural, and behavioral physiology*, 2004, **190**, (7), pp. 515–21

3 Vanderelst, D., Holderied, M.W., Peremans, H.: 'Sensorimotor model of obstacle avoidance in echolocating bats.', *PLoS computational biology*, 2015, **11**, (10), pp. e1004484

4 Vanderelst, D., Steckel, J., Boen, A., Peremans, H., Holderied, M.W.: 'Place recognition using batlike sonar', *eLife*, 2016, **5**, pp. e14188

5 Barchi, J.R., Knowles, J.M., Simmons, J.A.: 'Spatial memory and stereotypy of flight paths by big brown bats in cluttered surroundings', *Journal of Experimental Biology*, 2013, **216**, (6), pp. 1053–1063

6 Rihaczek, A.W.: 'Principles of high-resolution radar'. (New York: McGraw-Hill, 1969)

7 Blacknell, D., Griffiths, H.D., editors. 'Radar Automatic Target Recognition (ATR) and Non-Cooperative Target Recognition (NCTR)'. (Stevenage, UK: Institution of Engineering and Technology, 2013)

8 Griffiths, H.D., Baker, C.J., Adamy, D.: 'Stimson's Introduction to Airborne Radar'. 3rd ed. (Stevenage, UK: Institution of Engineering and Technology, 2014)

9 Baker, C.J., Griffiths, H.D., Balleri, A. 'Biologically inspired waveform diversity'. In: Gini, F., De.Maio, A., Patton, L., editors. Waveform Design and Diversity for Advanced Radar Systems. vol. 22 of *Radar, Sonar, Navigation and Avionics*. (Institution of Engineering and Technology, 2012. pp. 149–172

10 Saillant, P.A., Simmons, J.A., Dear, S.P., McMullen, T.A.: 'A computational model of echo processing and acoustic imaging in frequency-modulated echolocating bats: The spectrogram correlation and transformation receiver', *The Journal of the Acoustical Society of America*, 1993, **94**, (5), pp. 2691–2712

11 Simon, R., Knörnschild, M., Tschapka, M., Schneider, A., Passauer, N., Kalko, E.K.V., et al.: 'Biosonar resolving power: echo-acoustic perception of surface structures in the submillimeter range.', *Frontiers in physiology*, 2014, **5**, pp. 64

12 Simmons, J.A., Ferragamo, M., Moss, C.F., Stevenson, S.B., Altes, R.A.: 'Discrimination of jittered sonar echoes by the echolocating bat, eptesicus fuscus: The shape of target images in echolocation', *Journal of Comparative Physiology A*, 1990, **167**, (5), pp. 589–616

13 Simmons, J.A., Saillant, P.A., Wotton, J.M., Haresign, T., Ferragamo, M.J., Moss, C.F.: 'Composition of biosonar images for target recognition by echolocating bats', *Neural Networks*, 1995, **8**, (7-8), pp. 1239–1261

14 Schmidt, S.: 'Perception of structured phantom targets in the echolocating bat, megadermalyra', *The Journal of the Acoustical Society of America*, 1992, **91**, (4), pp. 2203–2223

15 Rihaczek, A.W.: 'Radar resolution of ideal point scatterers', *IEEE Transactions on Aerospace and Electronic Systems*, 1996, **32**, (2), pp. 842–845

16 Matsuo, I., Kunugiyama, K., Yano, M.: 'An echolocation model for range discrimination of multiple closely spaced objects: transformation of spectrogram into the reflected intensity distribution', *The Journal of the Acoustical Society of America*, 2004, **115**, (2), pp. 920–928

17 Wiegrebe, L.: 'An autocorrelation model of bat sonar', *Biological cybernetics*, 2008, **98**, (6), pp. 587–595

18 Sharma, N.S., Buck, J.R., Simmons, J.A.: 'Trading detection for resolution in active sonar receivers', *The Journal of the Acoustical Society of America*, 2011, **130**, (3), pp. 1272–1281

19 Georgiev, K., Balleri, A., Stove, A., Holderied, M.W. 'Baseband version of the bat-inspired spectrogram correlation and transformation receiver'. In: 2016 IEEE Radar Conference. (Philadelphia, USA, 2016.

20 Georgiev, K., Balleri, A., Stove, A., Holderied, M.W. 'Enhanced range resolution: comparison with the matched filter'. In: Balleri, A., Griffiths, H., Baker, C., editors. Biologically-Inspired Radar and Sonar: Lessons from Nature. (Stevenage, UK: IET, 2017.

21 Lyon, R.F., Katsiamis, A.G., Drakakis, E.M. 'History and future of auditory filter models'. In: Proceedings of 2010 IEEE International Symposium on Circuits and Systems. (Paris, France, 2010. pp. 3809–3812

22 Park, M., Allen, R.: 'Pattern-matching analysis of fine echo delays by the spectrogram correlation and transformation receiver', *The Journal of the Acoustical Society of America*, 2010, **128**, (3), pp. 1490–1500

23 Simmons, J.A., Gaudette, J.E., Warnecke, M. 'Biosonar inspired signal processing and acoustic imaging from echolocating bats'. In: Balleri, A., Griffiths, H., Baker, C., editors. Biologically-Inspired Radar and Sonar: Lessons from Nature. (Stevenage, UK: IET, 2017.

24 Stoica, P., Moses, R.L.: 'Spectral Analysis of Signals'. (Pearson Prentice Hall, 2005)

25 Zauderer, E.: 'Partial Differential Equations of Applied Mathematics'. (Wiley-Interscience, 2006)

26 Peremans, H., Hallam, J.: 'The spectrogram correlation and transformation receiver, revisited', *The Journal of the Acoustical Society of America*, 1998, **104**, (2), pp. 1101–1110

27 Georgiev, K., Balleri, A., Stove, A., Holderied, M. 'Bio-inspired two target resolution at radio frequencies'. In: 2017 IEEE Radar Conference (RadarConf). (Seattle, WA, USA, 2017. pp. 0436–0440